Supplement of Hydrol. Earth Syst. Sci., 24, 6047–6058, 2020
https://doi.org/10.5194/hess-24-6047-2020-supplement

Hydrology and Earth System Sciences
Open Access
EGU

Supplement of

Technical note: Mobile open dynamic chamber measurement of methane macroseeps in lakes

Frederic Thalasso et al.

Correspondence to: Frederic Thalasso (thalasso@cinvestav.mx) and Katey Walter Anthony (kmwalteranthony@alaska.edu)

Table S1: Notations.

Notation	Description	Units
A	Area	m^2
C	Gas concentration	$g\ m^{-3}$
d	Diameter	m
F	Gas flux	$g\ m^{-2}\ s^{-1}$
g	Standard gravity	$m\ s^{-2}$
M	Mass	g
P	Pressure	atm
Q	Gas flowrate	$m^3\ s^{-1}$
R	Universal gas constant	$L\ atm\ mol^{-1}\ K^{-1}$
T	Temperature	K
V	Gas volume	m^3
$\%_{CH4}$	Volume percentage of CH_4 in bubbles	%
θ	Response time	s
ρ	Volumetric density	$kg\ m^{-3}$
Subscripts		
P	Purge	
B	Bubble or ebullition	
D	Detector	
C	Chamber	
ATM	Atmospheric	
t	Time	

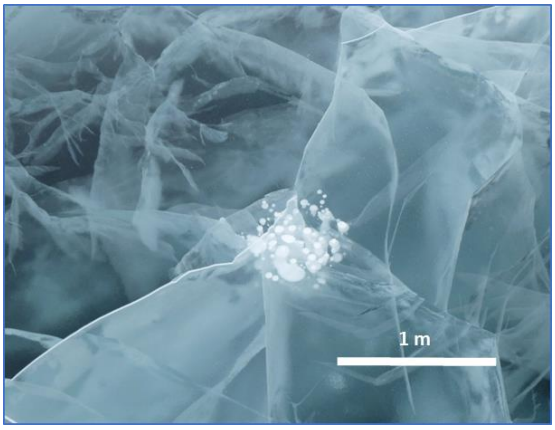

Figure S1. Methane bubbles trapped in the ice of an arctic lake, illustrating that ebullition occurs repeatedly in specific locations (Credit: A. Sepulveda-Jauregui, F. Thalasso).

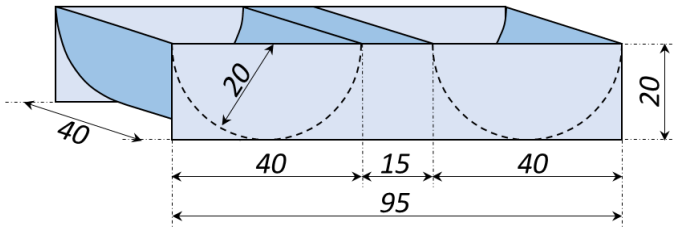

Figure S2. Dimension of the prototype built and used in the present work. Darker and lighter blue colors indicate three independent aluminum foils welded together. Dimensions are in cm.

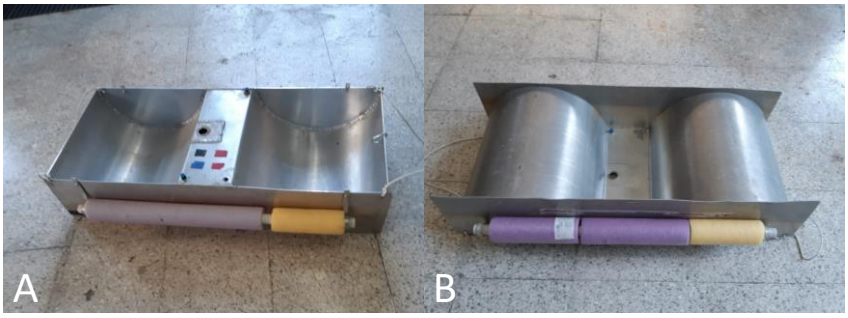

Figure S3. Superior (A) and inferior (B) view of the chamber hull with lateral floats added for improved stability.

Movie S1. Methane seeps; general and closeup views. Available at: Thalasso, Frederic (2020), "Esieh lake seepage HESS", Mendeley Data, V1, doi: 10.17632/fnr3mkxmk9.1

S1. Response time and data interpretation

The concentration read by the detector has a certain delay, due to the gas residence time from the chamber to the detector. However, if the detector is close to the chamber and the tubing of a reduced diameter, this time is very short; i.e., from 1.6 to 2.0 s in our case. However, even if it can be assumed that a bubble entering the chamber is immediately mixed within the chamber, the detectors have an inherent response time. This effect causes a certain delay and a buffer time, between the actual concentration read by the detector (C_D) and C_C. To take this delay into account a standard mixing model can be used (Eq. S12), where θ is the response time of the system

$$C_C = \left(\frac{dC_D}{dt} \cdot \theta\right) + C_D \quad \text{(S1)}$$

In Eq. (S1), θ was determined from experimental data, using several step C_D increases observed in the field. The adjustment was done through excel, minimizing the Root Mean Square Error (RMSE) between experimental C_D data and Eq. (S2), where $C_{D,0}$ is the initial reading of the detector (at time 0), and C_C is the actual concentration in the chamber.

$$C_D = C_{D,0} + \left[(1 - \exp(-t/\theta)) * (C_C - C_{D,0})\right] \quad \text{(S2)}$$

After C_C was determined, Eq. (5) was used to determine instantaneous F along the transects. Alternatively, Eq. (6) was used to determined mean flux over a transect section. In the case of instantaneous F, during transects, and despite the relatively high signal to noise ratio of detectors used; i.e., ratio of the mean to the standard deviation, F was subject to a significant noise, and a first data smoothening of C_C was necessary, followed by a second smoothening of dC_C/dt (Eq. S7). In both cases we opted for a pondered smoothening described by Eq. S3, where X´ is the smoothened variable X, in this case C_C or dC_C/dt.

$$X'_t = 0.1 \cdot X_{t-2} + 0.2 \cdot X_{t-1} + 0.4 \cdot X_t + 0.2 \cdot X_{t+1} + 0.1 \cdot X_{t+2} \quad \text{(S3)}$$

As it will be shown in the Results and Discussion section, peak fluxes were detected, which corresponded to step increases of C_C (ΔC_C), caused by bubbles reaching the chamber. These abrupt increases offer a unique opportunity to quantify the CH_4 mass content of the bubbles (M_B). It should be noticed that since these step increases were observed in a few seconds, the amount of CH_4 lost through detector extraction or entering the chamber can be neglected over that short time, as far a as single and clear increase was observed. Thus, M_B was determined during the field experiment according to Eq. (S4).

$$M_B = \Delta C_C \cdot V_C \quad \text{(S4)}$$

From M_B, the volume of the bubbles (V_B) and their equivalent spherical diameter (d_B) at atmospheric pressure were determined, assuming that the CH_4 content in the bubbles ($\%_{CH4}$) is known, according to Eq. (S5) and (S6), respectively.

$$V_B = \frac{M_B}{16} \cdot \frac{R \cdot T}{P} \cdot \frac{1}{\%_{CH4}} \quad \text{(S5)}$$

$$d_B = 2 \cdot \sqrt[3]{\frac{3 \cdot V_B}{4 \cdot \pi}} \quad \text{(S6)}$$

where 16 is the molecular weight of CH_4 (g), R is the universal gas constant (L atm mol^{-1} K^{-1}), T is the temperature (K) and P is the atmospheric pressure (atm).

Since bubble volume and diameters are important for mass transfer determination during their migration to the lake surface, the actual bubble volume (V'_B) at a given depth (D) within the water column is given by Eq. (S7).

$$V'_B = V_B \cdot \frac{P}{\frac{(\rho \cdot g \cdot D)}{101{,}325} + P} \quad \text{(S7)}$$

where ρ is the water volumetric mass density (kg m^{-3}), g is the standard gravity (m s^{-2}), and 101,325 is the conversion factor from Pa to atm.

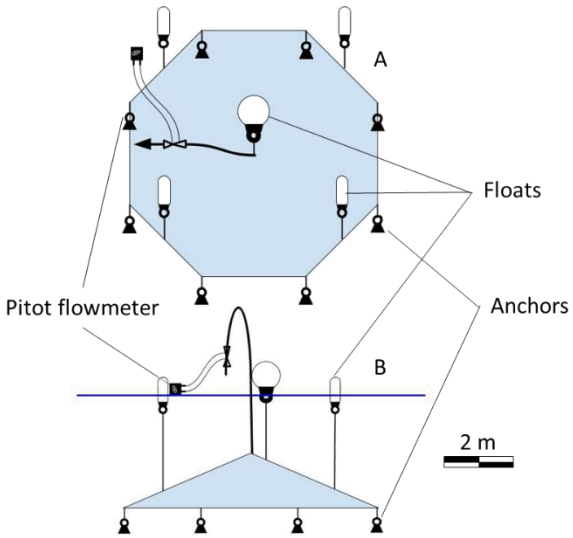

Figure S4. Conceptual sketch of the bubble trap used at Esieh Lake; (A) top view, (B) front view.

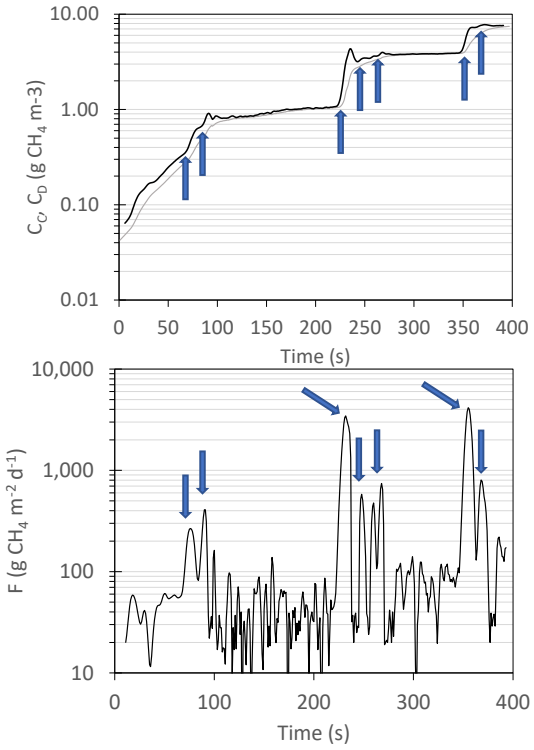

Figure S5. Additional example of; (A) C_D (grey solid line) and C_C (black solid line) measured during a transect, and (B) instantaneous flux computed from these concentrations. Blue arrows show when large bubbles were captured by the chamber. Please note the logarithmic scales.

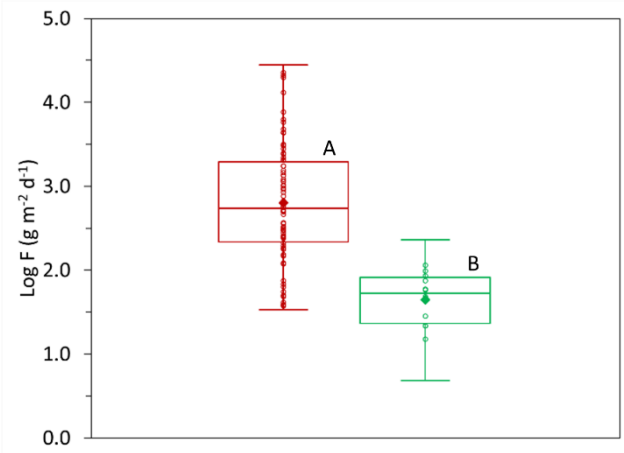

Figure S6. Box and whiskers showing statistical distribution of fluxes measured with the MOD chamber (A, n = 74) and the diffusive component of these fluxes (B, n = 14; see text for details). Boxes show interquartile range and median, whiskers represent minimum and maximum, open circles show raw data and filled diamonds represent arithmetic mean.

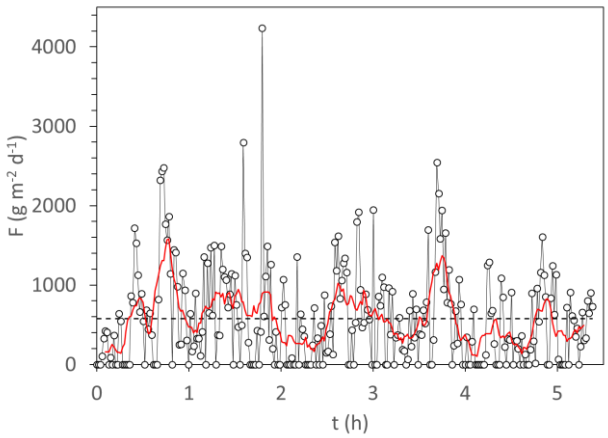

Figure S7. Flux measured by the bubble trap. Each discrete value is the average of 1 minute of continuous measurement. Horizontal discontinuous line shows the mean flux while red continuous line shows 10 minutes moving average of *F* data.

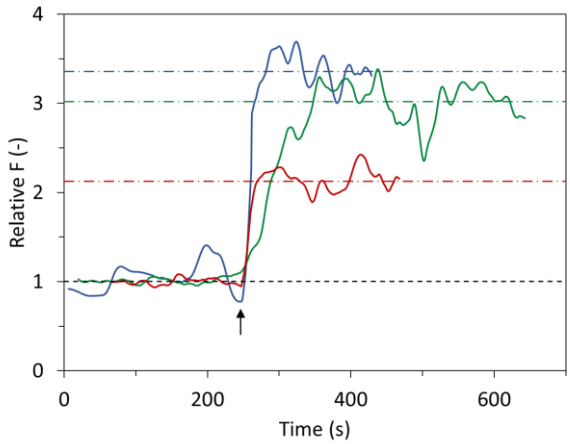

Figure S8: Relative fluxes observed with the MOD chamber, under stationary position (left of the arrows) and under motion. Data are presented in relative units, one being the flux observed in stationary position. Horizontal dot-dashed lines represent the mean fluxes during motion.

Table S2: Comparison of four methods with a potential to be used in lake seepage.

	Bubble trap	Duc et al. (2020)	Hydroacoustic	MOD Chamber
Large seeps	Yes	Potentially Yes	Potentially Yes	Yes
Diffusive flux	No	Yes	No	Yes
Mobility	No	No	Yes	Yes
Autonomous	No	Yes	No	No
Field effort	Important	Moderate	Low	Low
Data processing effort	Low	Moderate	High	Moderate
Cost range (US$)	Low-cost	Low-cost (un.)	50000[(1)]	10000-50000[(2)]

[1]Cost excluding video camera and mounting hardware; [2]Cost of the detector (the cost of the chamber assembly was about 300 US$ in material). un.: undisclosed.